

Efficiency of electrical manipulation on two-dimensional topological insulators

M. Pang and X. G. Wu

SKLSM, Institute of Semiconductors, Chinese Academy of Sciences, Beijing 100083, China

We investigate the efficiency of electrical manipulation on two-dimensional topological insulators by considering a lateral potential superlattice on the system. The electronic states under various conditions are examined carefully. It is found that the dispersion of the mini-band and the electron distribution in the potential well region display an oscillatory behavior as the potential strength of the lateral superlattice increases. The probability of finding an electron in the potential well region can be larger or smaller than the average as the potential strength varies. This indicates that the electric manipulation efficiency on two-dimensional topological insulators is not as high as expected, which should be carefully considered in designing a device application that bases on two-dimensional topological insulators. These features can be attributed to the coupled multiple-band nature of the topological insulator model. In addition, it is also found that these behaviors are not sensitive to the gap parameter of the two-dimensional topological insulator model.

PACS numbers: 73.21.Cd, 73.22.Dj

I. INTRODUCTION

Topological insulator has received widespread attentions in recent years because of its exotic electronic properties which suggest wonderful prospects both in the fundamental study and industrial applications [1–4]. Its novel feature lies on the observation that when it is of a finite size it has a linearly dispersive surface states (edge states in the two-dimensional system case) in the bulk gap [5–7]. The robustness of the surface states against disorder scattering makes topological insulator a promising new member of materials useful in the future information technology. In practical applications, electric manipulation of the carriers by voltage gates provides a basic important mechanism for the functioning of the devices. It thus becomes a crucial task is to learn how to control the behavior of electrons in topological insulators using electric fields. Various research concerning this issue have been done in the literature [8–19]. If the edges where the edge states localize can be created by electric voltage gates, namely, carriers in the system can be confined spatially by electric potential, it would greatly enhance the utilization of topological insulators as a building block of future devices. Actually, such design has been proposed [11] where the possibility of edges created by voltage gate is implicitly assumed without a serious and careful scientific justification.

Theoretically, the effective model put forward in Reference [20] has been widely used to describe the two-dimensional (2D) topological insulator [8–11, 15, 21–28]. In this model, one deals with a coupled two-component system (more generally, when the spin-orbit interaction is considered, it is a four-component system). The model resembles the Dirac equation describing a Dirac fermion which is known to exhibit the Klein tunneling phenomenon [29] and consequently a potential barrier may be unable to confine the fermion motion spatially.

Therefore, it will be interesting and meaningful to examine the influence of a spatially defined potential on the 2D topological insulator, especially the confinement

of electron wave functions induced by the externally applied potential. The present paper addresses this very important problem. We simplify the issue by considering a lateral potential superlattice structure made of a 2D topological insulator with spatially periodic, square shaped, electric potential barriers created by electric gate voltage. The single-electron energy dispersion and wave function will be calculated. The spatial dependence of wave function will be investigated when the lateral superlattice potential is varied.

The paper is organized as follows: In section II, the theoretical formulation is presented. Section III contains our calculated results and their discussions. Finally, in the last section, a summary is provided.

II. FORMULATION AND CALCULATION

The 2D topological insulator is modelled by the following well-known Hamiltonian [20]

$$\begin{pmatrix} h(\mathbf{k}) & 0 \\ 0 & h^*(-\mathbf{k}) \end{pmatrix}, \quad (1)$$

where $\mathbf{k} = (k_x, k_y)$. $h(\mathbf{k}) = \epsilon(\mathbf{k}) + \sum_{\alpha} d_{\alpha}(\mathbf{k})\sigma_{\alpha}$ with σ_{α} the Pauli matrix. $\epsilon(\mathbf{k}) = C - D(k_x^2 + k_y^2)$, $d_1 = Ak_x$, $d_2 = Ak_y$, and $d_3 = M - B(k_x^2 + k_y^2)$. A , B , C , D , and M are parameters determined by the structure of the quantum well [20]. The parameter C gives the zero point of energy and in this paper we can safely set it to zero for simplicity. When there is no coupling between spins (not the true spin, just for labeling convenience [20]), the lower 2×2 block $h^*(-\mathbf{k})$ and the upper block $h(\mathbf{k})$ are decoupled. They have the same energy spectrum and the corresponding wave functions are connected via an unitary transformation of time reversal operator. Thus in this paper we will limit ourselves to the analysis of upper block $h(\mathbf{k})$ only.

The topological insulator is in the xy plane, and the lateral potential superlattice is assumed to be along the

x axis and uniform in the y direction. The Hamiltonian describing the lateral superlattice is assumed to be given by $H = h(\mathbf{k}) + V(x)$. The potential $V(x)$ is diagonal and periodic in x . For simplicity, the square barrier potential is assumed. In one unit cell $x \in [0, L]$, $V(x) = 0$ for $x \in [R/2, L - R/2]$, and $V(x) = V_0$ otherwise. L is the period of the lateral superlattice and R is the width of the potential barrier in one unit cell. The lateral superlattice could be implemented by periodically depositing metal strips on the surface of the 2D topological insulator with the help of modern lithography technology. The barrier potential height can be varied by adjusting the bias voltage applied to the metal strips. The 2D topological insulator model is derived from a multiple band envelope function model [20]. Thus the assumption of a diagonal $V(x)$ is reasonable and consistent with the model, actually, similar kind of potential profile has been used in graphene [30].

The system is translational invariant in the y direction, and $k_y = p_y/\hbar$ is a good quantum number. But because of the presence of potential $V(x)$, there is no translational invariance in the x direction, and we follow the Peierls substitution to replace k_x in Equation (1) by the differential operator $-i\partial_x$. The explicit form of the Hamiltonian is thus as follows.

$$H = \begin{pmatrix} M + d_+ k^2 + V(x) & Ak_- \\ Ak_+ & -M + d_- k^2 + V(x) \end{pmatrix}, \quad (2)$$

with $d_+ = -(B + D)$, $d_- = B - D$, $k^2 = k_+ k_-$, $k_+ = -i\partial_x + ik_y$, and $k_- = -i\partial_x - ik_y$.

The wave function of the above Hamiltonian can be written as

$$\psi(x, y) = \frac{e^{ik_y y}}{\sqrt{L_y}} e^{iq_x x} \begin{pmatrix} u^u(x) \\ u^l(x) \end{pmatrix}, \quad (3)$$

with L_y the system size in the y direction and q_x the mini-band wave vector. $u^u(x) = u^u(x + L)$ and $u^l(x) = u^l(x + L)$ give the upper and lower components of the periodic part of the wave function. The wave vector q_x should be limited to the first Brillouin zone $q_x \in [-\pi/L, \pi/L]$. In the present paper, the plane wave expansion approach is used and sufficient number of plane waves are used to achieve the necessary accuracy for the energy levels. The wave function $u^s(x)$ can be written as $u^s(x) = L^{-1/2} \sum_n c_n^s e^{i2\pi n x/L}$ where s stands for u and l , respectively. The wave function $u^s(x)$ is normalized to unity in one unit cell.

The model for the 2D topological insulator contains many parameters. In the present paper, we will mainly consider the influence of the gap parameter M , as its sign has a profound effect on the electronic property when the 2D topological insulator has a finite size [20, 21]. The numerical values of other parameters A , B , and D are taken from reference [20]. The influence of the strength of superlattice potential V_0 will also be studied.

III. RESULTS AND DISCUSSIONS

In the absence of periodic potential, the bulk 2D topological insulator approximately has two bands [20]. The introduction of the lateral superlattice potential $V(x)$ leads to a multiple energy band structure. The eigen energy of the Hamiltonian H becomes $E_i(q_x, k_y)$ with i the band index. Extensive numerical works are carried out and qualitatively the same results are obtained. In the following we will show calculated results for a typical case of $L = 20$ nm and $R = L \times 0.5123456$. The ratio R/L is chosen to avoid possible length commensurate artifact and other ratios are also used.

It is found that, as V_0 increases (decreases), each band energy $E_i(q_x, k_y)$ increases (decreases) as a whole, roughly with an amount $V_0 R/L$, the averaged potential energy in one unit cell. Furthermore, for a given V_0 , if one takes the averaged potential $V_0 R/L$ as the energy zero point, then the m -th band above or below this averaged potential energy will approximately has its largest expansion coefficient $|c_n^s|$ at $|n| \sim |m|$ ($n = 0, \pm 1, \pm 2, \dots$). $|c_n^s|^2$ is shown in Figure 1, for a typical case of $q_x = 0.01$ nm $^{-1}$ and $k_y = 0$ with $M = -6.86$ meV. An almost linear dependence can be obviously seen. This shows that the bands near the averaged potential are more “ground state” like as it is less oscillatory compared to the bands more far away from the averaged potential. It is interesting to point out that when the sign of M changes, the behavior shown in Figure 1 is qualitatively the same, despite the fact that when $M > 0$ there is no edge state when the system is of a finite size.

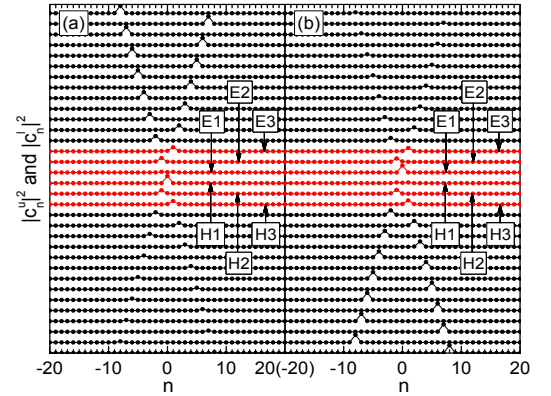


FIG. 1: (Color online) Square of the Fourier expansion coefficients $|c_n^u|^2$ (panel (a)) and $|c_n^l|^2$ (panel (b)) of wave functions for energy levels near the averaged potential $V_0 R/L$. $L = 20$ nm, $q_x = 0.01$ nm $^{-1}$, $k_y = 0$, $V_0 = 0.1$ eV, and $M = -6.86$ meV. The coefficients are shown as dots and lines connecting the dots are guide to the eye. For clarity, the coefficients for different energy levels are shifted vertically in the order of descending energy from top to bottom of the figure.

In this paper, we assume that the number of electrons in the 2D topological insulator will not be strongly af-

ected by the introduction of lateral superlattice potential. This approximation is consistent with the assumption of diagonal addition of the superlattice potential. If the fermi energy is near the band gap of the bulk 2D topological insulator which is taken as the energy zero point, then in the presence of the lateral superlattice potential the fermi energy should be close to the averaged potential. Thus in this paper we will focus on the bands near the averaged potential. For convenience we will label six bands near the averaged potential as $E1$, $E2$, $E3$, $H1$, $H2$ and $H3$, respectively (see Figure 1).

In Figure 2(a), we show the energy dispersion along the q_x direction in the first Brillouin zone ($[-\pi/L, \pi/L]$) for different values of V_0 and $k_y = 0$. In Figure 2(b), the

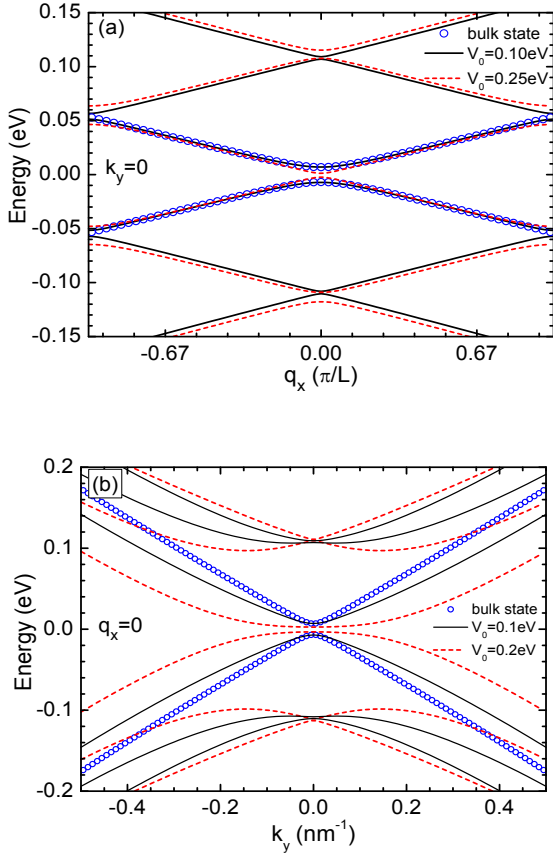


FIG. 2: (Color online) (a) The energy dispersion along the q_x direction in the first Brillouin zone of the lateral superlattice with $k_y = 0$. The averaged potential energy $V_0 R/L$ is subtracted from each energy level. The black solid line is for $V_0 = 0.1$ eV and the red dashed line is for $V_0 = 0.25$ eV. The open circles show the energy dispersion of the bulk state with no shift. (b) The energy levels versus k_y with the averaged potential energy subtracted for $q_x = 0$. The black solid line is for $V_0 = 0.1$ eV and the red dashed line is for $V_0 = 0.2$ eV. The open circles show the energy dispersion of the bulk state.

energy dispersion along the k_y direction is shown with $q_x = 0$. In each energy dispersion, the averaged potential

energy $V_0 R/L$ is subtracted. The bulk bands are also shown in Figure 2 as open symbols. When V_0 is small, the shape of bands $E1$ and $H1$ are close to the bulk bands as expected. We wish to point out that when the sign of M is reversed, the energy dispersion is qualitatively unchanged.

The energy dispersion changes in a rather complicated way when the barrier potential V_0 changes. In Figure 3, six energy levels are shown as a function of V_0 , with the average potential subtracted, for various values of q_x and a fixed $k_y = 0$. One can clearly see that all bands display an oscillatory behavior. There are three critical values of the potential V_0 at which the $E1$ and $H1$ bands ($E2$ and $E3$, $H2$ and $H3$) touch each other when $q_x = k_y = 0$. The oscillation amplitude will be smaller and no touching point exists when $q_x \neq 0$ or $k_y \neq 0$.

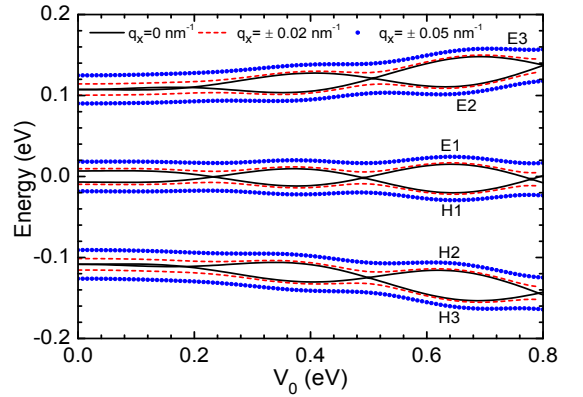


FIG. 3: (Color online) Energy levels versus V_0 the lateral superlattice barrier potential amplitude for various values of q_x and a fixed $k_y = 0$. The averaged potential energy is subtracted from each energy level. Curves with opposite sign of q_x are identical.

Next, we study the spatial dependence of wave functions. The system considered is uniform along the y direction, therefore we only need to investigate the probability distribution along the x direction. The total distribution, for a specific band, can be written as $|\Psi(x)|^2 = |u^u(x)|^2 + |u^l(x)|^2$ contributed from the upper and lower components of the corresponding wave function. Figure 4 shows the probability distribution for various value of q_x and k_y with a fixed $V_0 = 0.2$ eV. The well/barrier regions are indicated by two vertical lines in Figure 4. Figure 4(a) is for the $E1$ band and Figure 4(b) for the $H1$ band. It can be seen that, for the $E1$ band, the amplitude of wave function in the middle well region ($R/2 < x < L - R/2$) is larger than that in the barrier region ($0 < x < R/2$ and $R/2 < x < L$). But for the $H1$ band, the amplitude of wave function is larger in the barrier region.

It is interesting to note that the energy of $E1$ and $H1$ bands is about 0.1 eV, both below the barrier potential $V_0 = 0.2$ eV. On the other hand, the distribution shows that the $E1$ band behaves like a state in the well, while

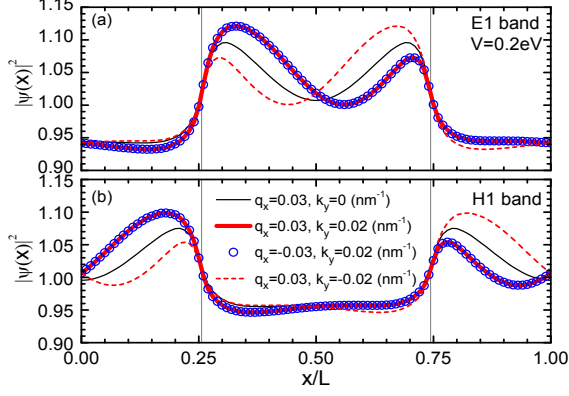


FIG. 4: (Color online) The spatial dependence of the total wave function in one lateral superlattice unit cell. (a) The total wave function of E1 band and (b) that of H1 band.

the *H1* band behaves like a state in the barrier, if we view them in a traditional single band picture. In the single band case, when the band energy is below the barrier of a superlattice potential, the wave function should be more confined in the well region. The result shown in Figure 4 indicates that a state whose energy is below the barrier could become “localized” in the well region or in the barrier region. This resembles the case of above-barrier states in a semiconductor superlattice [31–34]. This effect is not unexpected, as in the present study, we deal with a two-band model with a strong inter-band coupling.

As shown in Figure 4, electronic states with $k_y = 0$ have a symmetrical distribution about the center of the unit cell $x = L/2$. This symmetry will be destroyed if $k_y \neq 0$. However, the distribution of a state with $k_y = k_y^0 \neq 0$ and the distribution of a state with $k_y = -k_y^0$ are connected by a reflection transformation about the center of the unit cell. By making the reflection transformation, one obtains the distribution for $k_y = -k_y^0$ from the distribution for $k_y = k_y^0$ and vice versa. This symmetry about the distribution is due to the symmetry of the model Hamiltonian that $h^*(k_x, k_y) = h(k_x, -k_y)$.

Next, we study how the probability distribution (the wave function) changes when the lateral superlattice potential V_0 changes. This task becomes easier if we introduce the notion of probability distribution integrated over the well region in a unit cell $P_w = P_w^u + P_w^l$ with $P_w^u = \int_{R/2}^{L-R/2} |u^u(x)|^2 dx$ and $P_w^l = \int_{R/2}^{L-R/2} |u^l(x)|^2 dx$. Similarly, we also introduce P_b the probability distribution integrated over the barrier region in an unit cell. In Figure 5, we show the total P_w for the *E1* and *H1* bands for various values of q_x , k_y and M . It is clear that, as the barrier potential V_0 increases, the probability distribution in the well displays an oscillatory behavior around 0.5 the homogenous value. When $q_x = 0$, the oscillation of P_w shows abrupt changes at several values of V_0 (see Figure 5(a) and also Figure 5(d)). When $q_x \neq 0$, these

abrupt changes becomes smoother.

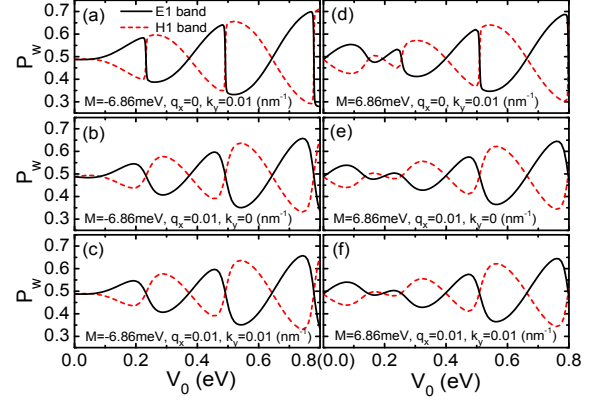


FIG. 5: (Color online) The wave function integrated in the well region P_w versus V_0 for various values of q_x and k_y . The solid curves are for the E1 band and dashed curves are for the H1 band. In (a), (b), and (c) $M = -6.86$ meV and in (d), (e), and (f) $M = 6.86$ meV. In (a) and (d), $q_x = 0$, $k_y = 0.01$ nm $^{-1}$. In (b) and (e), $q_x = 0.01$ nm $^{-1}$, $k_y = 0$. In (c) and (f), $q_x = 0.01$ nm $^{-1}$, $k_y = 0.01$ nm $^{-1}$.

The integrated probability distribution for the *E2*, *E3*, *H2*, and *H3* bands are shown in Figure 6 for $q_x = 0.01$ nm $^{-1}$, $k_y = 0$ and two values of M . The oscillatory be-

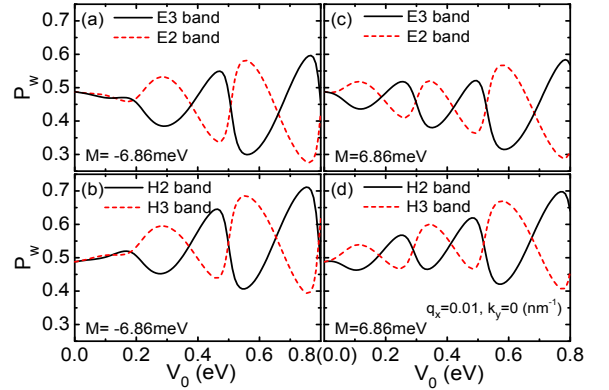


FIG. 6: (Color online) The wave function integrated in the well region P_w versus V_0 for $q_x = 0.01$ nm $^{-1}$ and $k_y = 0$. Panels (a) and (c) are for E2 and E3 bands, panels (b) and (d) are for H2 and H3 bands. In (a) and (b) $M = -6.86$ meV and in (c) and (d) $M = 6.86$ meV.

havior is similar to that of *E1* and *H1* bands except that the oscillation is slightly slantwise to the homogeneous distribution. States with even higher/lower energies are also investigated and similar results are found. This result is consistent with that in Reference [19], where the author found that the spin polarization oscillates across the boundary of a step-function electrical potential on the surface of a three dimensional topological insulator and

is not confined by the potential due to the Klein paradox. By examining Figure 5 and 6, one observes that the amplitude of the oscillation is not strong and this indicates that the effectiveness of gating on top of a 2D topological insulator is limited. As we have mentioned, this is due to the coupled two-band nature intrinsic to the system. Moreover, it should be pointed out that the oscillatory pattern can be modified dramatically when a different set of topological insulator parameters [21] is used.

It is well-known that, when the effective model for the 2D topological insulator is applied to a stripe geometry system, the existence of the nontrivial edge states requires that the bulk bands must be inverted, i.e., $M < 0$ [21]. When all parameters except M are unchanged, the model with negative M and positive M have completely different behavior when applied to the stripe system. In Figure 5 and 6, we compare P_w calculated with a negative M and a positive one. The left panels are for the negative M case and the right panels are for the positive M case. In the case of positive M , one observes that the number of oscillations increases. However, it is clear that there is no significant difference between two cases.

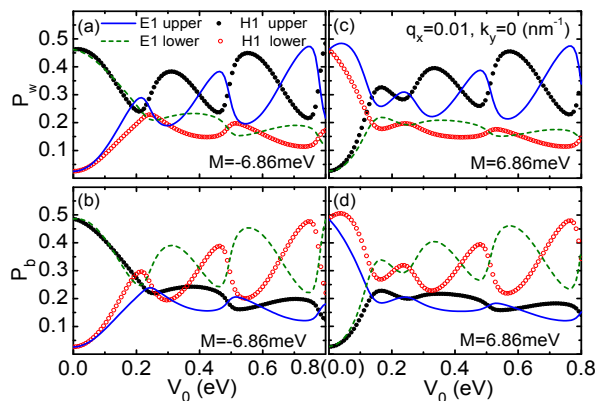


FIG. 7: (Color online) Panels (a) and (c) show the wave function integrated in the well region P_w versus V_0 , for the upper and lower components of the wave function. Panels (b) and (d) show the wave function integrated in the barrier region versus V_0 for both upper and lower components. Only the E1 and H1 bands represented. $q_x = 0.01 \text{ nm}^{-1}$ and $k_y = 0$. In (a) and (b) $M = -6.86 \text{ meV}$ and in (c) and (d) $M = 6.86 \text{ meV}$.

As the lateral superlattice studied in this paper is a coupled two-band system, we have evaluated the prob-

ability distribution for each component of a state. In Figure 7, the integrated probability distribution (wave function) is shown for the upper and lower component of wave function separately. The integral is performed either inside the potential well region (Figures 7(a) and 7(c)) or in the barrier region (Figures 7(b) and 7(d)). Only the results for the E1 and H1 bands are presented. In the left panels $M < 0$, and in the right panels $M > 0$. $q_x = 0.01 \text{ nm}^{-1}$ and $k_y = 0$. One observes that the two components both display oscillatory behavior.

In the case of $M < 0$ (Figures 7(a) and 7(b)), when V_0 is small, P_w and P_b of the H1 band mainly consists of the upper component, and for the E1 band they are dominated by the lower component. As V_0 increases, the difference between two components becomes small. In contrast, when $M > 0$ (Figures 7(c) and 7(d)) and V_0 is small, the E1 band is mainly contributed from the upper component and the H1 band is dominated by the lower component. More calculations show that when q_x and k_y becomes large, the contribution to P_w and P_b from upper and lower components will become nearly the same, even in the region of small V_0 .

IV. SUMMARY

In summary, we have investigated theoretically the properties of electronic states of a lateral superlattice made of a 2D topological insulator. The dispersion of mini-band and the electron wave function in the potential well region are found to display an oscillatory behavior as the potential strength of the lateral superlattice increases. The probability of finding an electron in the potential well region can be larger or smaller than the average as the potential strength varies. This indicates that the electrical confining effect in two-dimensional topological insulators is not high and one should be careful with the idea of creating boundaries using gate voltage in device design. These features are different from that in a single-band Kronig-Penney model, and can be attributed to the coupled-multiple-band nature of the 2D topological insulator model.

Acknowledgments

This work was partly supported by NSF and MOST of China.

-
- [1] S.-C. Zhang, *Physics* **1**, 6 (2008).
 - [2] X.-L. Qi and S.-C. Zhang, *Physics Today* **63**, 33 (2010).
 - [3] M. Z. Hasan and C. L. Kane, *Rev. Mod. Phys.* **82**, 3045 (2010).
 - [4] J. E. Moore, *Nature* **464**, 194 (2010).
 - [5] M. König, S. Wiedmann, C. Brüne, A. Roth, H. Buh-

- mann, L. W. Molenkamp, X.-L. Qi, and S.-C. Zhang, *Science* **318**, 766 (2007).
- [6] D. Hsieh, D. Qian, L. Wray, Y. Xia, Y. S. Hor, R. J. Cava, and M. Z. Hasan, *Nature* **452**, 970 (2008).
- [7] J. G. Analytis, R. D. McDonald, S. C. Riggs, J.-H. Chu, G. S. Boebinger, and I. R. Fisher, *Nat. Phys.* **6**, 960 (2010).

- (2010).
- [8] L. B. Zhang, K. Chang, X. C. Xie, H. Buhmann, and L. W. Molenkamp, *New Journal of Physics* **12**, 083058 (2010).
 - [9] L. B. Zhang, F. Zhai, and K. Chang, *Phys. Rev. B* **81**, 235323 (2010).
 - [10] Z.-F. Jiang, R.-L. Chu, and S.-Q. Shen, *Phys. Rev. B* **81**, 115322 (2010).
 - [11] L. B. Zhang, F. Cheng, F. Zhai, and K. Chang, *Phys. Rev. B* **83**, 081402 (2011).
 - [12] F. Dolcini, *Phys. Rev. B* **83**, 165304 (2011).
 - [13] R. Citro, F. Romeo, and N. Andrei, *Phys. Rev. B* **84**, 161301 (2011).
 - [14] D. Zhang and C. S. Ting, *Phys. Rev. B* **85**, 115434 (2012).
 - [15] P. Michetti, J. C. Budich, E. G. Novik, and P. Recher, *Phys. Rev. B* **85**, 125309 (2012).
 - [16] J. Wang, X. Chen, B.-F. Zhu, and S.-C. Zhang, *Phys. Rev. B* **85**, 235131 (2012).
 - [17] F. Romeo, R. Citro, D. Ferraro, and M. Sassetti, *Phys. Rev. B* **86**, 165418 (2012).
 - [18] T. Yokoyama, A. V. Balatsky, and N. Nagaosa, *Phys. Rev. Lett.* **104**, 246806 (2010).
 - [19] J.-H. Gao, J. Yuan, W.-Q. Chen, Y. Zhou, and F.-C. Zhang, *Phys. Rev. Lett.* **106**, 057205 (2011).
 - [20] B. A. Bernevig, T. L. Hughes, and S.-C. Zhang, *Science* **314**, 1757 (2006).
 - [21] B. Zhou, H.-Z. Lu, R.-L. Chu, S.-Q. Shen, and Q. Niu, *Phys. Rev. Lett.* **101**, 246807 (2008).
 - [22] J. Li, R.-L. Chu, J. K. Jain, and S.-Q. Shen, *Phys. Rev. Lett.* **102**, 136806 (2009).
 - [23] K. Chang and W.-K. Lou, *Phys. Rev. Lett.* **106**, 206802 (2011).
 - [24] V. Krueckl and K. Richter, *Phys. Rev. Lett.* **107**, 086803 (2011).
 - [25] M. J. Schmidt, E. G. Novik, M. Kindermann, and B. Trauzettel, *Phys. Rev. B* **79**, 241306 (2009).
 - [26] E. G. Novik, P. Recher, E. M. Hankiewicz, and B. Trauzettel, *Phys. Rev. B* **81**, 241303 (2010).
 - [27] V. Krueckl and K. Richter, *Phys. Rev. B* **85**, 115433 (2012).
 - [28] Y. Takagaki, *Phys. Rev. B* **85**, 155308 (2012).
 - [29] N. Dombey and A. Calogeracos, *Physics Reports* **315**, 41 (1999).
 - [30] M. R. Masir, P. Vasilopoulos, and F. M. Peeters, *Journal of Physics: Condensed Matter* **22**, 465302 (2010).
 - [31] S. Colak and K. Shahzad, *Phys. Rev. B* **38**, 9667 (1988).
 - [32] F. C. Zhang, N. Dai, H. Luo, N. Samarth, M. Dobrowolska, J. K. Furdyna, and L. R. Ram-Mohan, *Phys. Rev. Lett.* **68**, 3220 (1992).
 - [33] F. C. Zhang, H. Luo, N. Dai, N. Samarth, M. Dobrowolska, and J. K. Furdyna, *Phys. Rev. B* **47**, 3806 (1993).
 - [34] S. M. Tseng, Y. F. Chen, Y. T. Cheng, C. W. Hsu, Y. S. Huang, and D. Y. Lin, *Phys. Rev. B* **64**, 195311 (2001).